GEOPHYSICS, VOL. 81, NO. 4 (JULY-AUGUST 2016); P. T175–T188, 11 FIGS., 2 TABLES.
10.1190/GEO2015-0362.1

An effective anisotropic poroelastic model for elastic wave propagation in finely layered media

Asiya M. Kudarova[1], Karel N. van Dalen[2], and Guy G. Drijkoningen[2]

ABSTRACT

Mesoscopic-scale heterogeneities in porous media cause attenuation and dispersion at seismic frequencies. Effective models are often used to account for this. We have developed a new effective poroelastic model for finely layered media, and we evaluated its impact focusing on the angle-dependent attenuation behavior. To enable this, an exact solution was obtained for the response of a periodically layered medium to a surface point load using Floquet's theory. We compared this solution with that of the new model and the equivalent viscoelastic vertical transverse isotropic medium available from existing literature. We have observed that the quasi-P (qP) wave dispersion and attenuation was predicted with high accuracy by the new effective poroelastic model. For the quasi-S (qS) wave, the effective poroelastic model provides a perceptibly better prediction of the attenuation, resulting in closer to the exact waveforms. The qS-wave attenuation is underestimated by the effective viscoelastic model, whereas for the qP-wave, the model gives accurate predictions in all cases except for highly permeable weak-frame media.

INTRODUCTION

Horizontally layered models are commonly used for the analysis of wave propagation in reservoir rocks and sediments. This is a compromise between a relatively accurate representation of heterogeneities in rocks and simplicity of computations. Assuming lateral homogeneity is reasonable because the variations in properties in the direction normal to the layering are typical for most reservoir rocks and sediments. Layered models allow us to study the effects of local inhomogeneities at the macroscopic scale. The layers can represent mesoscopic-scale heterogeneities when their thicknesses are much larger than the typical pore and grain sizes, but smaller than the wavelength of a propagating wave. Mesoscopic heterogeneities are known to cause strong dispersion and attenuation of seismic waves due to the subwavelength scale wave-induced fluid flow (Müller et al., 2010). The attenuation is particularly strong when a medium is saturated with different fluids with a large contrast in compressibility (White et al., 1975; Carcione and Picotti, 2006).

The commonly used equations describing wave propagation in fluid-saturated media are Biot's (1962) equations of poroelasticity. This theory predicts one S- and two P-waves in a macroscopically homogeneous medium. It is widely accepted that Biot's theory underestimates observed attenuation and dispersion of elastic waves (Johnston et al., 1979; Winkler, 1985; Gist, 1994). One of the reasons is a violation of the assumption of uniform saturation with a single fluid. Inhomogeneities in solid-frame properties also cause attenuation. Many models for wave propagation in heterogeneous porous media were developed to address this effect. Each model proposes an attenuation mechanism that is based on certain assumptions. These assumptions are related, among other things, to the scale of the heterogeneities and their distributions, and the frequency range of interest. Depending on the scale of observations, different models are used to study wave attenuation and dispersion. Attenuation due to dissipation at the pore scale is described by a squirt-flow mechanism (O'Connell and Budiansky, 1977; Mavko and Nur, 1979; Palmer and Traviola, 1980; Dvorkin and Nur, 1993). Differences in fluid saturation between thin compliant pores and larger stiffer ones, the presence of thin cracks, different shape and orientation of the pores, as well as distribution of immiscible fluids in a pore cause attenuation and dispersion due to local or squirt flow. This mechanism usually plays a role at ultrasonic frequencies. At seismic frequencies, another attenuation mechanism caused by the subwavelength-scale fluid flow due to the presence of mesoscopic-scale heterogeneities plays a role. This mechanism is not captured by

Manuscript received by the Editor 5 July 2015; revised manuscript received 21 December 2015; published online 17 June 2016.
[1]Formerly Delft University of Technology, Department of Geoscience and Engineering, Delft, The Netherlands; presently Shell Global Solutions International B.V., Rijswijk, The Netherlands. E-mail: asiya.kudarova@shell.com.
[2]Delft University of Technology, Department of Geoscience and Engineering, Delft, The Netherlands. E-mail: k.n.vandalen@tudelft.nl; g.g.drijkoningen@tudelft.nl.

Biot's theory, which accounts for a global (wavelength-scale) flow attenuation mechanism. Because gas, oil, and water are often present in the rocks and sediments as mesoscopic-scale patches, multiple models are being developed that describe attenuation of seismic waves in such heterogeneous media.

One of the pioneering works on seismic attenuation caused by the wave-induced fluid flow is the work of White et al. (1975), in which a periodically layered porous medium was considered, and a frequency-dependent plane-wave modulus was derived for normal wave incidence. Similar but differently derived moduli were reported in other publications (Norris, 1993; Brajanovski and Gurevich, 2005; Vogelaar and Smeulders, 2007). Some other models of effective P-wave moduli make use of a frequency-dependent branching function that connects the low- and high-frequency limits (e.g., Johnson, 2001). Krzikalla and Müller (2011) introduce an effective vertical transverse isotropic (VTI) medium to describe propagation of quasi-P (qP) and quasi-S (qS) waves at different angles. In their model, the low- and high-frequency elastic moduli from poroelastic Backus averaging by Gelinsky and Shapiro (1997) are connected by a frequency-dependent function — the effective P-wave modulus of White et al. (1975) for periodic layering and normal incidence. For a randomly layered medium with a small fluctuation of parameters, the frequency-dependent function can be derived from Gelinsky et al. (1998). With the approach used by Krzikalla and Müller (2011), any model where a plane-wave modulus for P-wave propagation normal to the layering is derived can be extended for arbitrary angle of incidence. Another approach to compute the frequency-dependent coefficients of the effective VTI medium numerically was proposed by Carcione et al. (2011). The resulting effective medium in both approaches is governed by the equations of a viscoelastic VTI medium, and has five complex-valued frequency-dependent stiffnesses. This means that the fluid-to-solid relative motion is not explicitly present in the model. Instead, the information about attenuation caused by the interaction of the fluid and solid phases at the subwavelength scale is included in the frequency dependence of the effective stiffnesses. Furthermore, this effective model does not incorporate a slow P-wave on the macroscopic scale, as predicted by Biot's theory. On the one hand, this is advantageous from the computational point of view as the presence of the slow wave requires a very fine meshing in 3D numerical simulations. On the other hand, Biot's global flow mechanism — macroscopic attenuation due to viscous forces between fluid and solid phases — is not captured in the equations of viscoelasticity, which may be disadvantageous even in the seismic frequency range (Kudarova et al., 2013).

In this paper, we combine the effective constants from the poroelastic Backus averaging (Gelinsky and Shapiro, 1997) and the method proposed by Krzikalla and Müller (2011). We use the effective P-wave moduli introduced by Kudarova et al. (2013). This results in the effective stiffnesses of an effective poroelastic VTI medium governed by Biot's equations. This effective medium accounts for the macroscopic (Biot's global flow) attenuation via the effective inertia and viscous terms used in Biot's equations, and for the mesoscopic (subwavelength scale) attenuation via the frequency dependence of the effective stiffnesses. We consider wave propagation in a 2D half-space, subject to a point source at the surface. Solutions to this problem are obtained for the effective viscoelastic model mentioned above and for the newly derived poroelastic model. As a reference, an exact analytical solution is obtained with the use of Floquet's (1883) theory. The responses predicted by all three solutions are compared.

The paper is structured as follows: First, Biot's equations are briefly reviewed. Second, the equations for the effective viscoelastic model are presented. Then, the effective poroelastic model is introduced. The numerical examples follow, where predictions by all models are compared based on the responses in the time domain. The discussion of the results and conclusions finalizes the paper.

THEORETICAL MODELS

In this section, we present the equations of Biot's theory, followed by the equations of the effective viscoelastic model and the ones of the effective poroelastic model. The exact solution for a periodically layered medium governed by Biot's equations is given in Appendix A.

Biot's theory

Biot's (1962) equations of motion read

$$\tau_{ij,j} = \rho \ddot{u}_i + \rho_f \ddot{w}_i, \tag{1}$$

$$-p_{,i} = \rho_f \ddot{u}_i + \frac{\alpha_{ij}\rho_f}{\phi}\ddot{w}_j + \eta r_{ij}\dot{w}_j. \tag{2}$$

Throughout this paper, a comma in the subscript denotes a spatial derivative, an overdot denotes a time derivative, and the summation convention for repeated indices is assumed. The following notations are used: ρ_f, ρ_s are the fluid and solid grain densities, respectively; ϕ is the porosity, and the total density $\rho = (1-\phi)\rho_s + \phi\rho_f$; $\alpha_{ij} = \alpha_\infty \delta_{ij}$, where α_∞ is the tortuosity, δ_{ij} is the Kronecker delta, and η is the fluid viscosity; τ_{ij} are the elements of the total stress tensor, p is the fluid pressure, and u and w are the displacements of the solid phase and the relative fluid-to-solid displacement multiplied by ϕ, respectively. Tensor $\mathbf{r} = \mathbf{k_0^{-1}}$, where the elements of $\mathbf{k_0}$ are the permeabilities k_{ij}, and for the isotropic case $k_{ij} = k_0\delta_{ij}$. The high-frequency correction to Biot's viscous damping factor is commonly adopted to account for dynamic effects, resulting in the dynamic permeability $\hat{k}_0 = k_0(\sqrt{1 + i\omega M/(2\omega_B)} + i\omega/\omega_B)^{-1}$ (and consequently, a temporal convolution operator in equation 2), where M is the parameter that depends on the pore geometry, permeability, and porosity (Johnson et al., 1987). The real part of the square root is taken greater than zero. Throughout the paper, we assume $M = 1$; it was shown to be accurate for several pore types (Smeulders et al., 1992). Biot's critical frequency $\omega_B = \phi\eta/(k_0\alpha_\infty\rho_f)$ separates the low-frequency regime from the regime, where inertial and viscous forces dominate.

Throughout the paper, a circumflex accent $\hat{f}$ above a quantity stands for frequency-wavenumber dependence (or frequency only, if there is no wavenumber dependence). The Fourier transform is applied for transforming to the frequency-wavenumber domain:

$$\hat{f}(k_x,z,\omega) = \int_{-\infty}^{\infty}\int_{-\infty}^{\infty} \exp(-i\omega t + ik_x x) f(x,z,t)\,dt\,dx. \tag{3}$$

The inverse Fourier transform is given by

$$f(x,z,t)=\frac{1}{2\pi^2}\int_0^\infty \mathrm{Re}\left(\int_{-\infty}^{\infty}\hat{f}(k_x,z,\omega)\times\exp(\mathrm{i}\omega t-\mathrm{i}k_x x)dk_x\right)d\omega. \quad (4)$$

Only positive frequencies are considered because the negative frequency components do not provide information independent of the positive components. We study propagation of the plane waves in the $x-z$ plane, where x is the horizontal direction and z is the vertical direction.

The stress-strain relations for an isotropic medium read

$$\begin{aligned}\tau_{xx}&=E_1u_{x,x}+(E_1-2\mu)u_{z,z}+E_2(w_{x,x}+w_{z,z}),\\ \tau_{zz}&=(E_1-2\mu)u_{x,x}+E_1u_{z,z}+E_2(w_{x,x}+w_{z,z}),\\ \tau_{xz}&=\mu(u_{x,z}+u_{z,x}),\\ -p&=E_2(u_{x,x}+u_{z,z})+E_3(w_{x,x}+w_{z,z}),\end{aligned} \quad (5)$$

where the coefficients are defined as follows (Biot, 1962):

$$\begin{aligned}&E_1=P+2Q+R,\quad E_2=(Q+R)/\phi,\quad E_3=R/\phi^2,\\ &P=\frac{\phi K_m+(1-\phi)K_f(1-\phi-K_m/K_s)}{\phi+K_f(1-\phi-K_m/K_s)/K_s}+\frac{4}{3}\mu,\\ &Q=\frac{\phi K_f(1-\phi-K_m/K_s)}{\phi+K_f(1-\phi-K_m/K_s)/K_s},\\ &R=\frac{\phi^2K_f}{\phi+K_f(1-\phi-K_m/K_s)/K_s}.\end{aligned} \quad (6)$$

In the above equations, K_s, K_f, and K_m are the bulk moduli of the solid grains, fluid, and the drained frame, respectively, and μ is the shear modulus of the drained frame.

In the frequency-wavenumber domain, we look for plane-wave solutions of the equations 1 and 2 in the form

$$\hat{\mathbf{u}}=(\hat{U}_x,\hat{U}_z,\hat{W}_x,\hat{W}_z)^{\mathrm{T}}\exp(-\mathrm{i}k_z z). \quad (7)$$

In the isotropic case, the P- and S-wave motions are decoupled. The corresponding dispersion relations are obtained by introducing the displacement potentials $[\hat{\phi}_s,\hat{\psi}_s,\hat{\phi}_f,\hat{\psi}_f]=[\hat{\Phi}_s,\hat{\Psi}_s,\hat{\Phi}_f,\hat{\Psi}_f]\times\exp(-\mathrm{i}k_z z)$, where

$$\begin{aligned}\hat{u}_x&=-\mathrm{i}k_x\hat{\phi}_s-\hat{\psi}_{s,z},\quad \hat{w}_x=-\mathrm{i}k_x\hat{\phi}_f-\hat{\psi}_{f,z},\\ \hat{u}_z&=\hat{\phi}_{s,z}-\mathrm{i}k_x\hat{\psi}_s,\quad \hat{w}_z=\hat{\phi}_{f,z}-\mathrm{i}k_x\hat{\psi}_f.\end{aligned} \quad (8)$$

Substitution of these relations into equations 1 and 2 leads to the dispersion equation

$$\{(E_1E_3-E_2^2)s^4-(\rho E_3+\hat{m}E_1-2\rho_f E_2)s^2+\rho\hat{m}-\rho_f^2\}\{\mu\hat{m}s^2-\rho\hat{m}+\rho_f^2\}=0. \quad (9)$$

In equation 9, $s=\sqrt{k_x^2+k_z^2}/\omega$ denotes slowness. The operator $\hat{m}=\rho_f\alpha_\infty/\phi+\hat{b}/(\mathrm{i}\omega\phi^2)$, where $\hat{b}=b_0\sqrt{1+\mathrm{i}\omega/(2\omega_B)}$ is the dynamic viscous factor (the real part of the square root is positive), and $b_0=\eta\phi^2/k_0$. The first brace term in equation 9 is a dispersion equation for P-waves, and the second one is that for S-waves.

Effective viscoelastic VTI model

We first introduce the equations for the effective viscoelastic model, and then, the additional parameters are defined to obtain the equations of motion for the effective poroelastic model, given in the next section. The effective VTI model for wave propagation in layered media at arbitrary angle was presented by Krzikalla and Müller (2011). This effective model makes use of the poroelastic Backus averaging (Gelinsky and Shapiro, 1997) and the effective plane-wave modulus obtained for a periodic 1D medium (White et al., 1975). The resulting equations in the effective medium are equations of elasticity with frequency-dependent coefficients. Throughout the paper, we refer to this model as the viscoelastic model.

The analysis of dispersion and attenuation predicted by this model for media with inhomogeneities in frame properties is carried out by Krzikalla and Müller (2011). In the current paper, we present the space-time domain responses of the effective medium to a surface point load. We discuss examples with inhomogeneities in solid frame and fluid properties. The equations used in this analysis are outlined below.

The equations of motion for the effective VTI viscoelastic model read

$$\begin{aligned}-\mathrm{i}k_x\hat{\tau}_{xx}+\hat{\tau}_{xz,z}&=-\omega^2\rho\hat{u}_x,\\ -\mathrm{i}k_x\hat{\tau}_{xz}+\hat{\tau}_{zz,z}&=-\omega^2\rho\hat{u}_z,\end{aligned} \quad (10)$$

where ρ is the density of the homogenized medium obtained by averaging over the layers 1 and 2 of the periodic cell: $\rho=\langle\rho(z)\rangle$. Throughout the paper, the angular brackets denote averaging over the layers in the periodic cell

$$\langle f\rangle=\frac{1}{L}\int_L f(z)dz. \quad (11)$$

The stress-strain relations for the effective viscoelastic VTI model read

$$\begin{aligned}\hat{\tau}_{xx}&=-\mathrm{i}k_x\hat{A}\hat{u}_x+\hat{F}\hat{u}_{z,z},\\ \hat{\tau}_{xz}&=\hat{D}(\hat{u}_{x,z}-\mathrm{i}k_x\hat{u}_z),\\ \hat{\tau}_{zz}&=-\mathrm{i}k_x\hat{F}\hat{u}_x+\hat{C}u_{z,z}.\end{aligned} \quad (12)$$

In the effective medium, the stiffnesses in the above equations are frequency dependent. The expressions for the effective stiffnesses $\hat{A}$, $\hat{F}$, $\hat{C}$, and $\hat{D}$ were obtained by Gelinsky and Shapiro (1997) in two limiting cases of relaxed and unrelaxed pore pressures (the expressions are given in Appendix C). These limits are referred to as quasistatic and no-flow limits, respectively. It is assumed that the fluid flow is independent of the loading direction (i.e., direction of wave propagation), and a single relaxation function connects the relaxed and unrelaxed limits of the effective stiffnesses. This function is based on a frequency-dependent modulus $\hat{c}(\omega)$, derived originally by White et al. (1975). The expression for $\hat{c}(\omega)$ is given in Appendix C. The normalized relaxation function reads

$$\hat{R}(\omega) = \frac{\hat{c}(\omega) - C^u}{C^r - C^u}, \tag{13}$$

where the superscripts r and u refer to the relaxed and unrelaxed limits, respectively. The effective stiffnesses then read

$$\{\hat{A}, \hat{C}, \hat{F}, \hat{D}\} = \{A, C, F, D\}^u - \hat{R}(\omega)(\{A, C, F, D\}^u - \{A, C, F, D\}^r). \tag{14}$$

It follows from equation 14 that $\hat{C} = \hat{c}(\omega)$. Because the shear modulus does not depend on the fluid pressure, it is the same in the relaxed and the unrelaxed cases, and the effective shear modulus $\hat{D}$ does not depend on frequency:

$$\hat{D} = D^u = D^r = \left\langle \frac{1}{\mu} \right\rangle^{-1}. \tag{15}$$

To obtain the dispersion equations of the effective viscoelastic VTI model, we look for the solution of equation 10 in the frequency-wavenumber domain in the form

$$(\hat{u}_x, \hat{u}_z) = (\hat{U}_x, \hat{U}_z)\exp(-\mathrm{i}k_z z). \tag{16}$$

Substituting this into equation 10 and taking into account equation 12 provides the following solutions of the dispersion equation:

$$\begin{aligned} k_{1z}^{\pm} &= \pm\sqrt{\frac{\epsilon_1 + \sqrt{\epsilon_2}}{2\hat{D}\hat{C}}},\quad k_{2z}^{\pm} = \pm\sqrt{\frac{\epsilon_1 - \sqrt{\epsilon_2}}{2\hat{D}\hat{C}}},\\ \epsilon_1 &= \rho(\hat{C}+\hat{D}) - (\hat{A}\hat{C} - 2\hat{D}\hat{F} - \hat{F}^2)k_x^2,\\ \epsilon_2 &= (\hat{A}^2\hat{C}^2 - 4(\hat{A}\hat{C}+\hat{F})\hat{D} - 2\hat{F}^2(\hat{A}\hat{C} - 2\hat{D}^2) + \hat{F}^3(4\hat{D}+\hat{F}))k_x^4 +\\ &\quad + 2\rho(\hat{F}(\hat{D}+\hat{C})(\hat{F}+2\hat{D}) + \hat{C}\hat{D}(2\hat{D}+\hat{A}) - \hat{A}\hat{C}^2)k_x^2 + \rho^2(\hat{C}-\hat{D})^2. \end{aligned} \tag{17}$$

The pairs of the wavenumbers $k_{1z,2z}^{\pm}$ correspond to upgoing and downgoing qP- and qS-waves. The amplitude ratios $\hat{U}_z/\hat{U}_x$ read

$$\left(\frac{\hat{U}_z}{\hat{U}_x}\right)_{1,2}^{\pm} = \frac{\rho\omega^2 - \hat{A}k_x^2 - \hat{D}(k_{1z,2z}^{\pm})^2}{(\hat{F}+\hat{D})k_x k_{1z,2z}^{\pm}}. \tag{18}$$

Effective poroelastic VTI model

In this section, we introduce the effective poroelastic model based on the poroelastic Backus averaging (Gelinsky and Shapiro, 1997) and the effective plane-wave moduli obtained for P-wave propagation at normal incidence in a periodically layered porous medium (Kudarova et al., 2013). These effective moduli result from using the boundary conditions at the interfaces of the periodic cell different from those used in White's et al. (1975) model. The no-flow condition is replaced with the pressure continuity condition, allowing fluid flow at the macroscopic scale. As a result, two additional plane-wave moduli are derived to describe the effective medium with Biot's equations. These effective moduli are used to define the effective stiffnesses $\hat{B}_6$, $\hat{B}_7$, and $\hat{B}_8$ (notation used as in Gelinsky and Shapiro, 1997) required to describe the effective poroelastic VTI model. Apart from the effective stiffnesses, the effective densities have to be defined. We use the results obtained by Molotkov and Bakulin (1999), who showed that the effective medium representing a stack of Biot's layers is a generalized transversely isotropic Biot's medium. In this poroelastic medium, the densities and the viscous terms in Biot's equations are defined differently in the x- and z-directions. The equations of motion read

$$\begin{aligned} -\mathrm{i}k_x\hat{\tau}_{xx} + \hat{\tau}_{xz,z} &= -\omega^2\hat{\rho}_x\hat{u}_x - \omega^2\hat{\rho}_{fx}\hat{w}_x,\\ -\mathrm{i}k_x\hat{\tau}_{xz} + \hat{\tau}_{zz,z} &= -\omega^2\rho_z\hat{u}_z - \omega^2\rho_{fz}\hat{w}_z,\\ \mathrm{i}k_x\hat{p} &= -\omega^2\hat{\rho}_{fx}\hat{u}_x - \omega^2\hat{m}_x\hat{w}_x,\\ -\hat{p}_{,z} &= -\omega^2\rho_{fz}\hat{u}_z - \omega^2\hat{m}_z\hat{w}_z, \end{aligned} \tag{19}$$

where the coefficients on the right side read (Molotkov and Bakulin, 1999)

$$\begin{aligned} \hat{\rho}_{fx} &= \frac{s_1\rho_{f1}\hat{m}_2 + s_2\rho_{f2}\hat{m}_1}{s_1\hat{m}_2 + s_2\hat{m}_1}, \quad \hat{m}_x = \left\langle \frac{1}{\hat{m}} \right\rangle^{-1},\\ \hat{\rho}_x &= \langle\rho\rangle - \frac{s_1 s_2(\rho_{f1} - \rho_{f2})^2}{s_1\hat{m}_2 + s_2\hat{m}_1},\\ \rho_z &= \langle\rho\rangle, \quad \rho_{fz} = \langle\rho_f\rangle, \quad \hat{m}_z = \langle\hat{m}\rangle. \end{aligned} \tag{20}$$

The indices 1 and 2 in equation 20 refer to the layers 1 and 2. The volume fractions of the layers are $s_1 = l_1/L$ and $s_2 = l_2/L$.

The stress-strain relations read

$$\begin{aligned} \hat{\tau}_{xx} &= -\mathrm{i}k_x\hat{A}\hat{u}_x + \hat{F}\hat{u}_{z,z} + \hat{B}_6(-\mathrm{i}k_x\hat{w}_x + \hat{w}_{z,z}),\\ \hat{\tau}_{zz} &= -\mathrm{i}k_x\hat{F}\hat{u}_x + \hat{C}\hat{u}_{z,z} + \hat{B}_7(-\mathrm{i}k_x\hat{w}_x + \hat{w}_{z,z}),\\ \hat{\tau}_{xz} &= \hat{D}(\hat{u}_{x,z} - \mathrm{i}k_x\hat{u}_z),\\ -\hat{p} &= -\mathrm{i}k_x\hat{B}_6\hat{u}_x + \hat{B}_7\hat{u}_{z,z} + \hat{B}_8(-\mathrm{i}k_x\hat{w}_x + \hat{w}_{z,z}). \end{aligned} \tag{21}$$

The frequency-dependent stiffnesses in equation 21 are defined in the same way as in the effective viscoelastic model, but the frequency dependence is incorporated via the effective plane-wave moduli obtained by Kudarova et al. (2013). These effective moduli are obtained from the solution of the 1D problem for the periodic cell consisting of two isotropic layers (see Figure 1a), where harmonic stress and pressure are applied to the outer edges of the cell normal to the layering. The layers are governed by Biot's equations 1 and 2 (with z-dependent field variables u_z, w_z, τ_{zz}, and p). The problem is solved in the frequency domain. In each layer, the displacements u_z and w_z are found as upgoing and downgoing plane waves (a fast and a slow P-wave), resulting in eight unknown amplitudes. These amplitudes are found from the following boundary conditions: continuity of the intergranular stress σ_{zz}, pore pressure p, displacements u_z and w_z at the interface between the layers, and continuity of the total stress τ_{zz} and pressure p at the outer edges of the cell. The strains $u_{z,z}$ and $w_{z,z}$ are found as the difference between the displacements at the outer edges of the unit cell, divided by the

cell width. This gives us the coefficients of the frequency-dependent symmetric compliance matrix $\hat{\alpha}_{ij}$:

$$\hat{u}_{z,z} = \hat{\alpha}_{11}\hat{\tau}_{zz} + \hat{\alpha}_{12}\hat{p},$$
$$\hat{w}_{z,z} = \hat{\alpha}_{12}\hat{\tau}_{zz} + \hat{\alpha}_{22}\hat{p}. \tag{22}$$

They are equated to the coefficients of the compliance matrix obtained from Biot's stress-strain relations (equation 5, for 1D case, with $k_x = 0$):

$$\hat{u}_{z,z} = \frac{1}{\hat{\Delta}}(\hat{E}_3\hat{\tau}_{zz} + \hat{E}_2\hat{p}),$$
$$\hat{w}_{z,z} = \frac{1}{\hat{\Delta}}(-\hat{E}_2\hat{\tau}_{zz} - \hat{E}_1\hat{p}), \qquad \hat{\Delta} = \hat{E}_1\hat{E}_3 - \hat{E}_2^2. \tag{23}$$

Then, the frequency-dependent elastic parameters $\hat{E}_1$, $\hat{E}_2$, and $\hat{E}_3$ are found, describing attenuation and dispersion due to wave-induced mesoscopic fluid flow in 1D periodically layered medium:

$$\hat{E}_1 = \frac{\hat{\alpha}_{22}}{\hat{\alpha}_{11}\hat{\alpha}_{22} - \hat{\alpha}_{12}^2}, \quad \hat{E}_2 = -\frac{\hat{\alpha}_{12}}{\hat{\alpha}_{11}\hat{\alpha}_{22} - \hat{\alpha}_{12}^2}, \quad \hat{E}_3 = \frac{\hat{\alpha}_{11}}{\hat{\alpha}_{11}\hat{\alpha}_{22} - \hat{\alpha}_{12}^2}. \tag{24}$$

The coefficients α_{ij} are computed numerically by solving a system of eight by eight linear algebraic equations corresponding to eight boundary conditions in the cell problem, mentioned above.

Following Krzikalla and Müller (2011), we introduce a branching function

$$\hat{R}_1(\omega) = \frac{\hat{E}_1(\omega) - C^u}{C^r - C^u} \tag{25}$$

to obtain the frequency-dependent effective moduli $\hat{A}$, $\hat{C}$, and $\hat{F}$:

$$\{\hat{A}, \hat{C}, \hat{F}\} = \{A, C, F\}^u - \hat{R}_1(\omega)(\{A, C, F\}^u - \{A, C, F\}^r). \tag{26}$$

As discussed above, the modulus $\hat{D}$ is not frequency dependent and is defined in equation 15. Note that $\hat{R}_1(\omega)$ is equivalent to $\hat{R}(\omega)$ (equation 13) when the frequency is much lower than Biot's critical frequency ω_B. The effective plane-wave modulus $\hat{E}_1$ is an extension of White's frequency-dependent modulus $\hat{c}(\omega)$ to higher frequencies, first proposed by Vogelaar and Smeulders (2007). Further generalization is proposed by Kudarova et al. (2013), where the no-flow boundary conditions at the outer edges of the unit cell are replaced by the pressure continuity condition, allowing the global flow to take place. This results in additional effective moduli $\hat{E}_2$ and $\hat{E}_3$ defined in equation 24, which are used to describe the effective Biot's medium.

By comparing the expressions for τ_{zz} and p in equation 5 (with incorporated frequency-dependent coefficients, $\hat{E}_1$, $\hat{E}_2$, and $\hat{E}_3$, introduced above) and equation 21, we can find out how the other moduli of the effective poroelastic VTI model should be chosen. First, it can be observed that

$$\hat{B}_7 = \hat{E}_2, \qquad \hat{B}_8 = \hat{E}_3. \tag{27}$$

Next, the effective coefficient $\hat{B}_6$ should be obtained. In the particular case when the shear modulus is constant throughout the layers, there is no anisotropy in the stiffness matrix of the effective poroelastic medium, and $\hat{B}_6 = \hat{B}_7 = \hat{E}_2$. Anisotropy remains in the viscous and inertia terms, according to their definition in equation 20. In general case, complying with the method used by Krzikalla and Müller (2011), the frequency dependence of $\hat{B}_6$ is specified using a second normalized relaxation function:

$$\hat{R}_2(\omega) = \frac{\hat{E}_2 - B_7^u}{B_7^r - B_7^u}. \tag{28}$$

The final expression for the effective modulus $\hat{B}_6$ then reads

$$\hat{B}_6 = B_6^u - \hat{R}_2(\omega)(B_6^u - B_6^r). \tag{29}$$

Now, all effective constants have been determined. For clarity, we underline that the effective poroelastic model incorporates the mesoscopic and the macroscopic attenuation mechanisms; the former is captured by the effective stiffnesses in equation 21, whereas the latter comes in through the effective terms defined in equation 20.

To obtain the dispersion equation of the effective poroelastic VTI model, we look for the solution of equation 21 in the form

$$\{\hat{u}_x, \hat{u}_z, \hat{w}_x, \hat{w}_z\} = \{\hat{U}_x, \hat{U}_z, \hat{W}_x, \hat{W}_z\}\exp(-\mathrm{i}k_z z). \tag{30}$$

Substitution of equation 30 into the stress-strain relations (equation 21) and the equations of motion (equation 19) gives the dispersion relation $\det(\mathbf{M}) = 0$ with solutions $k_z(k_x)$, where $\mathbf{M}$ is a matrix with coefficients given as

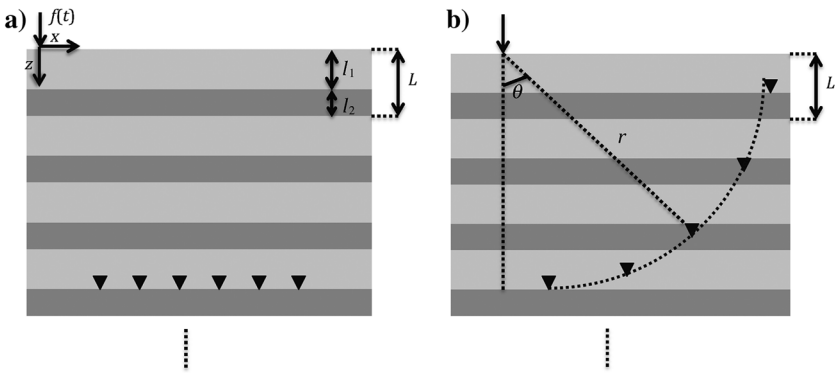

Figure 1. Point-force source at the top of the layered half-space and receivers (a) on a horizontal line below the source and (b) on the arc.

$$\mathbf{M}=\begin{bmatrix} \hat{A}k_x^2+\hat{D}k_z^2-\omega^2\hat{\rho}_x & (\hat{D}+\hat{F})k_xk_z & \hat{B}_6k_x^2-\omega^2\hat{\rho}_{fx} & \hat{B}_6k_xk_z \\ (\hat{F}+\hat{D})k_xk_z & \hat{C}k_z^2+\hat{D}k_x^2-\omega^2\rho_z & \hat{B}_7k_xk_z & \hat{B}_7k_z^2-\omega^2\rho_{fz} \\ -\hat{B}_6k_x^2+\omega^2\hat{\rho}_{fx} & -\hat{B}_7k_xk_z & -\hat{B}_8k_x^2+\hat{m}_x\omega^2 & -\hat{B}_8k_xk_z \\ -\hat{B}_6k_xk_z & -\hat{B}_7k_z^2+\omega^2\rho_{fz} & -\hat{B}_8k_xk_z & -\hat{B}_8k_z^2+\hat{m}_z\omega^2 \end{bmatrix}. \tag{31}$$

The matrix determinant $\det(\mathbf{M})=0$ provides the dispersion relation:

$$c_1k_z^6+c_2k_z^4+c_3k_z^2+c_4=0. \tag{32}$$

Explicit expressions for the coefficients c_i are not presented here for the sake of brevity; they can be expressed in terms of the elements of the matrix $\mathbf{M}$. The solution of equation 32 is

$$\begin{aligned} k_{1z}^{\pm}&=\pm\sqrt{\frac{a}{6c_1}-\frac{2}{3}\frac{3c_1c_3-c_2^2}{c_1a}-\frac{c_2}{3c_1}}, \\ k_{2z}^{\pm}&=\pm\sqrt{-(1-\mathrm{i}\sqrt{3})\frac{a}{12c_1}+2(1+\mathrm{i}\sqrt{3})\frac{3c_1c_3-c_2^2}{6c_1a}-\frac{c_2}{3c_1}}, \\ k_{3z}^{\pm}&=\pm\sqrt{-(1+\mathrm{i}\sqrt{3})\frac{a}{12c_1}+2(1-\mathrm{i}\sqrt{3})\frac{3c_1c_3-c_2^2}{6c_1a}-\frac{c_2}{3c_1}}, \end{aligned} \tag{33}$$

where

$$\begin{aligned} a=\Bigg(&12\sqrt{3(27c_1^2c_4^2-18c_1c_2c_3c_4+4c_1c_3^3+4c_2^3c_4-c_2^2c_3^2)c_1} \\ &-108c_4c_1^2+36c_1c_2c_3-8c_2^3\Bigg)^{1/3}. \end{aligned} \tag{34}$$

These vertical components of the wavenumbers correspond to the upgoing and downgoing fast qP-, the slow qP-, and the qS-waves.

RESULTS

In this section, we compare the space-time domain responses of three half-spaces subject to a surface point source (vertical stress component) and evaluate the performance of the effective models for media with different properties. The first half-space consists of periodically alternating layers, where each layer is governed by Biot's equations. The exact analytical solution presented in Appendix A is used to obtain the response in the frequency-wavenumber domain. The response in the space-time domain is obtained with the use of the inverse Fourier transform (equation 4). The second half-space is a homogeneous VTI medium governed by the equations of the effective viscoelastic VTI model outlined above, originally introduced by Krzikalla and Müller (2011). The third half-space is a homogeneous VTI medium governed by the equations of the effective poroelastic VTI model introduced in this paper.

Configuration

We consider a periodically layered half-space with the normal stress at the surface applied at some reference point $x=0$. The receivers are located on one horizontal line (Figure 1a) and on the arc of a circle with the radius r (Figure 1b). The latter configuration is instrumental to highlight angle-dependent effects. The sets of the material parameters are given in Table 1 (solid frame properties) and Table 2 (saturating fluids properties). The examples with rocks and water- and gas-saturated coarse sand were used by Gelinsky and Shapiro (1997). The properties of the coarse and medium sands originate from Turgut and Yamamoto (1990). The example with alternating layers of a water and CO_2-saturated sandstone were introduced by Carcione et al. (2011).

The boundary conditions at the top interface $z=0$ read

$$\tau_{zz}=f(t)\delta(x), \quad \tau_{xz}=0, \quad p=0. \tag{35}$$

For the effective VTI viscoelastic model, only the first two boundary conditions apply because the fluid pressure is not present in the equations of the viscoelastic model. For the function $f(t)$, a Ricker wavelet is used:

$$f(t)=f_0(1-2\pi^2f_R^2(t-t_0)^2)\exp(-\pi^2f_R^2(t-t_0)^2). \tag{36}$$

Table 1. Sets of material properties chosen for numerical examples.

Parameter	Notation	Units	Rock 1	Rock 2	Sandstone	Medium sand	Coarse sand
Density of solid grains	ρ_s	kg/m^3	2650	2650	2650	2650	2650
Bulk modulus of solid grains	K_s	GPa	40	40	40	36	36
Bulk modulus of frame	K_m	GPa	12.7	4.3	1.37	0.108	0.217
Porosity	ϕ	–	0.15	0.17	0.36	0.4	0.35
Permeability	k_0	m^2	10^{-13}	$2\cdot10^{-13}$	$1.6\cdot10^{-12}$	10^{-11}	10^{-10}
Shear modulus	μ	GPa	20.3	8.8	0.82	0.05	0.1
Tortuosity	α_∞	–	1	1	2.8	1.25	1.25
Biot's critical frequency (water)	$\frac{\omega_B}{2\pi}$	kHz	1500	850	80.3	5.1	0.445
Biot's critical frequency (CO_2)	$\frac{\omega_B}{2\pi}$	kHz	445	252	23.9	9.5	0.8
Biot's critical frequency (gas)	$\frac{\omega_B}{2\pi}$	kHz	107	60	5.7	2.3	0.2

In the above equation, f_0 is a constant scaling coefficient with the dimension of stress (Pa), f_R is the central frequency of the wavelet, and t_0 is an arbitrary time shift chosen, such that the dominant part of the wavelet lies within the positive domain $t > 0$; only the components that are infinitely small are left in the domain $t < 0$. In the examples, we compare the vertical components of the solid displacements u_z.

Numerical examples

First, we look at the response of a medium consisting of alternating water-saturated rocks 1 and 2. The receivers are located on a horizontal line at a vertical distance $z = 400$ m from the source, and the layer thicknesses are $l_1 = l_2 = 0.2$ m. The wavelet parameters are $f_R = 50$ Hz, $f_0 = 10^9$ Pa, and $t_0 = 0.022$ s. Because there is a variation in the shear modulus of the layers, the effective viscoelastic medium is a VTI medium, as well as the effective poroelastic medium. The exact solution describes the original layered medium. Time-domain responses are shown in Figure 2. In all the plots, the dashed black line corresponds to the solution predicted by the effective viscoelastic model, the solid black line corresponds to the exact analytical solution, and the solid gray line corresponds to the effective poroelastic model. In Figure 2, all three lines coincide; the effective models are in agreement with the exact solution for the qP- and qS-waves, as well as for the head wave that can be distinguished.

The second example is a medium consisting of sandstone layers with alternating water and CO_2 saturations, and the thicknesses of the layers are the same as in the previous example. This configuration is considered by Carcione et al. (2011), who report a good match between the dispersion and attenuation predictions by their numerical solution and the analytical solution of Krzikalla and Müller (2011). The shear modulus is constant throughout the layers, which means that the effective viscoelastic medium is isotropic resulting in decoupling between P- and S-wave motions. In this particular case, the qS-wave velocity in the effective viscoelastic model is equal to the S-wave velocity $v = \sqrt{\mu/\rho}$, where μ is a real-valued shear modulus and ρ is a real-valued effective density. Hence, the effective viscoelastic model does not predict any S-wave attenuation. However, the effective poroelastic model is not isotropic because of the anisotropy in the effective density terms (equation 19). Therefore, the qS-wave is attenuated in the effective poroelastic model and the exact solution. To observe this effect, the central frequency of the wavelet in this example is increased to 200 Hz and $t_0 = 0.0055$ s. The qP-wave waveforms are shown in Figure 3 and the qS-wave ones in Figure 4. It can be observed that the qP-waveforms are all in agreement (all lines coincide), but the qS-wave attenuation is underestimated by the effective models; with the effective viscoelastic model, it is underestimated to a greater extent, whereas the difference between the predictions by the effective poroelastic model and the exact solution is smaller.

In the effective poroelastic model, Biot's global flow mechanism causes qS-wave attenuation captured by the viscous terms in equation 19. This mechanism is not present in the effective viscoelastic model, which could result in different predictions as shown in Figure 4. However, the influence of Biot's global flow mechanism at this frequency range well below Biot's critical frequency (see Table 1) is probably small, which is confirmed by the fact that the predictions for the qP-waveforms match for all models. The observed differences in the qS-waveforms are likely to be related to the different description of the mesoscopic-scale attenuation mechanism in the models. In the viscoelastic model, there is no S-wave attenuation; in the poroelastic model, the mesoscopic-scale attenuation of the qS-wave is captured in the compressional motion, associated with the qS-wave. The difference between the effective poroelastic model qS-waveform and that of the exact solution is

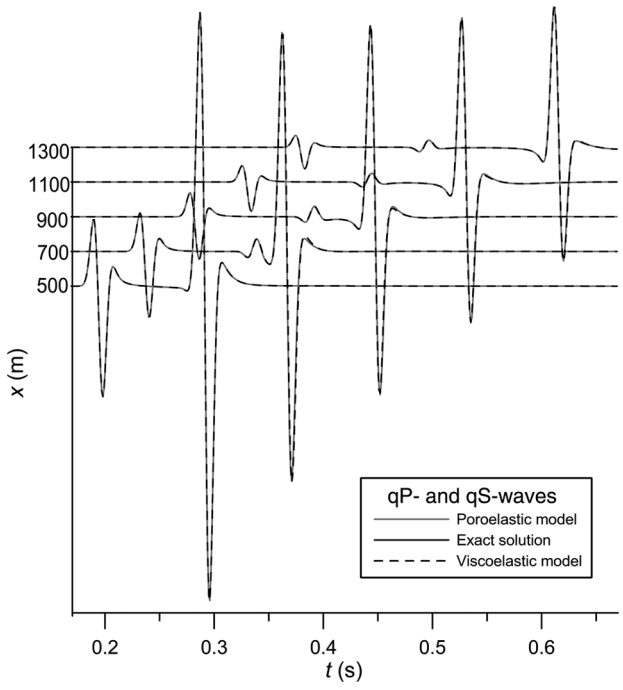

Figure 2. Time-domain response at a depth $z = 400$ m for different x. The medium consists of water-saturated alternating layers of rocks 1 and 2, $l_1 = l_2 = 0.2$ m, $f_R = 50$ Hz. All three lines coincide.

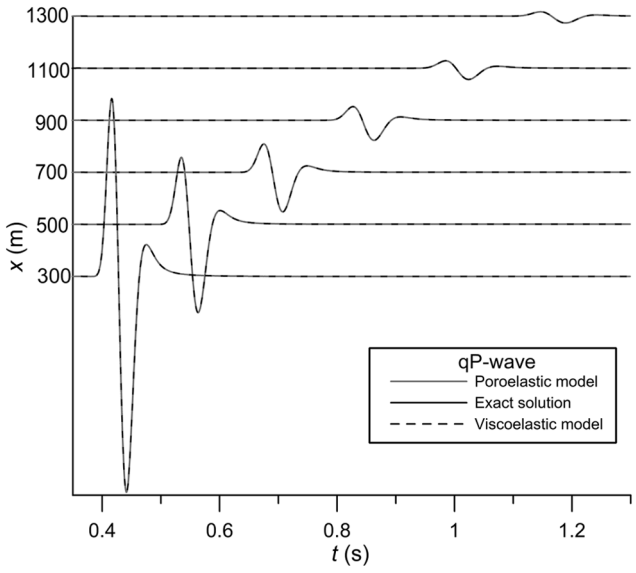

Figure 3. The qP-waveforms at a depth $z = 400$ m for different x. The medium consists of water- and CO_2-saturated sandstone layers, $l_1 = l_2 = 0.2$ m, $f_R = 200$ Hz. All three lines coincide.

probably due to more complicated fluid pressure distribution associated with the qS-wave (Wenzlau et al., 2010), which is not captured by the effective moduli derived for the 1D cell problem.

It was shown by Kudarova et al. (2013) that Biot's global flow mechanism is important for predictions of P-wave attenuation at seismic frequencies for highly permeable weak-frame media. In the next examples, we consider such media to compare the predictions of the three models considered in this paper for qP- and qS-waves. First, water-saturated alternating layers of medium sand

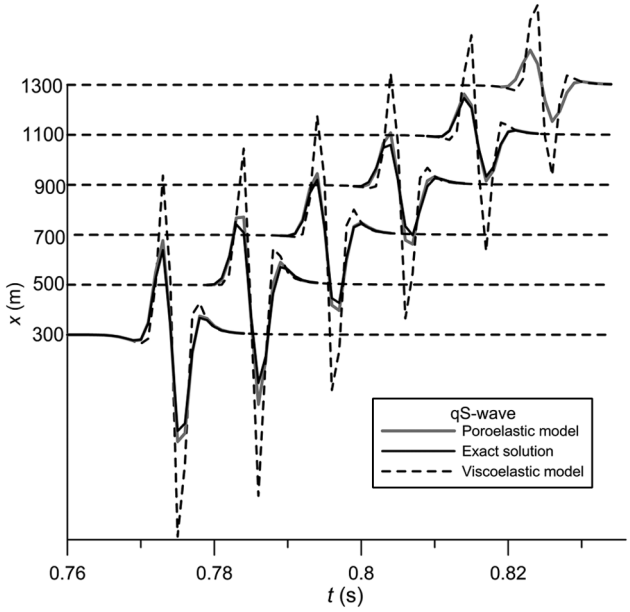

Figure 4. The qS-waveforms at a depth $z = 400$ m for different x. The medium consists of water- and CO_2-saturated sandstone layers, $l_1 = l_2 = 0.2$ m, $f_R = 200$ Hz. The actual arrival times are not shown here, the interval between the arrival times $t = 0.01$ s is chosen for visualization purposes.

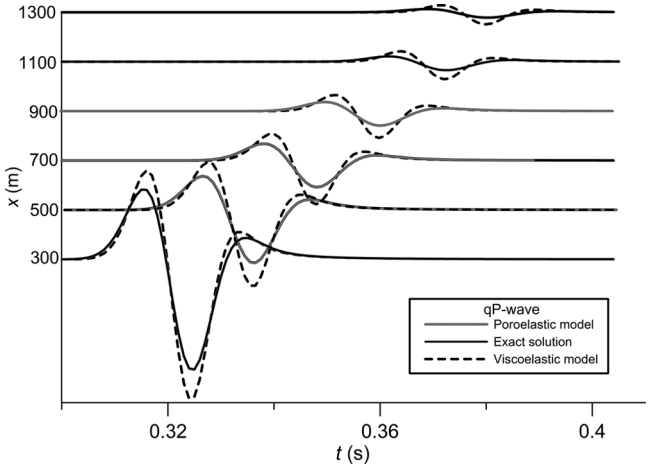

Figure 5. The qP-waveforms at a depth $z = 400$ m for different x. The medium consists of water-saturated medium and coarse sand, $l_1 = l_2 = 0.2$ m, $f_R = 50$ Hz. Solid gray and black lines coincide. The actual arrival times are not shown here, and the interval between the arrival times $t = 0.01$ s is chosen for visualization purposes.

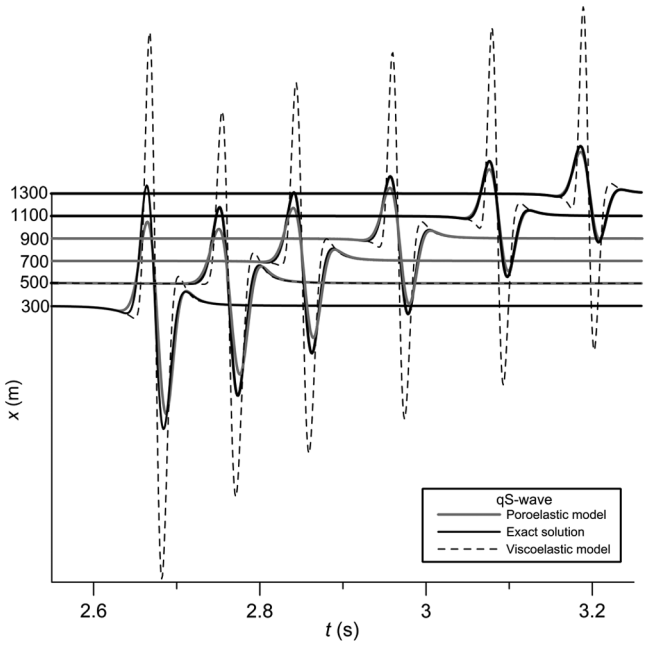

Figure 6. The qS-waveforms at a depth $z = 400$ m for different x. The medium consists of water-saturated medium and coarse sand, $l_1 = l_2 = 0.2$ m, $f_R = 50$ Hz. The actual arrival times are not shown here, and the interval between the arrival times $t = 0.1$ s is chosen for visualization purposes.

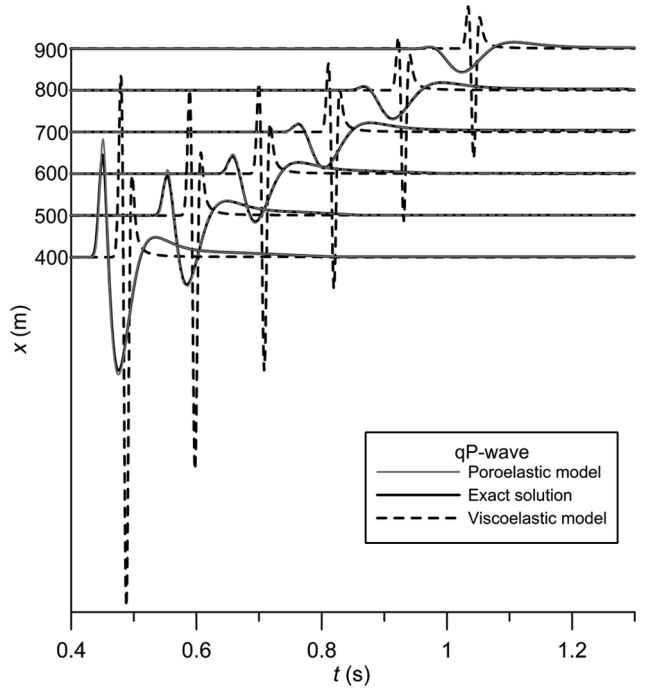

Figure 7. The qP-waveforms at a depth $z = 100$ m for different x. The medium consists of the layers of coarse sand, $l_1 = 0.09$ m (water saturated), $l_2 = 0.01$ m (gas saturated), $f_R = 50$ Hz. Each trace is multiplied by the corresponding propagation distance, and the traces predicted by the effective viscoelastic model are scaled by the factor 0.1.

and coarse sand are considered. The thicknesses of the layers are $l_1 = l_2 = 0.2$ m, and the receivers are located at a depth $z = 400$ m. The central frequency of the wavelet $f_R = 50$ Hz. It can be observed from the waveforms of the qP- (Figure 5) and qS-waves (Figure 6) that the effective viscoelastic model underestimates qP- and qS-waves attenuation. The effective poroelastic model predicts the same qP-waveforms as the exact solution, and its predictions for the qS-wave are closer to the exact solution than the predictions of the effective viscoelastic model. In this example, the effective viscoelastic model is also a VTI medium because there is a variation in the shear moduli of the layers. The P- and S-wave motions are coupled; therefore, the qS-wave is not lossless.

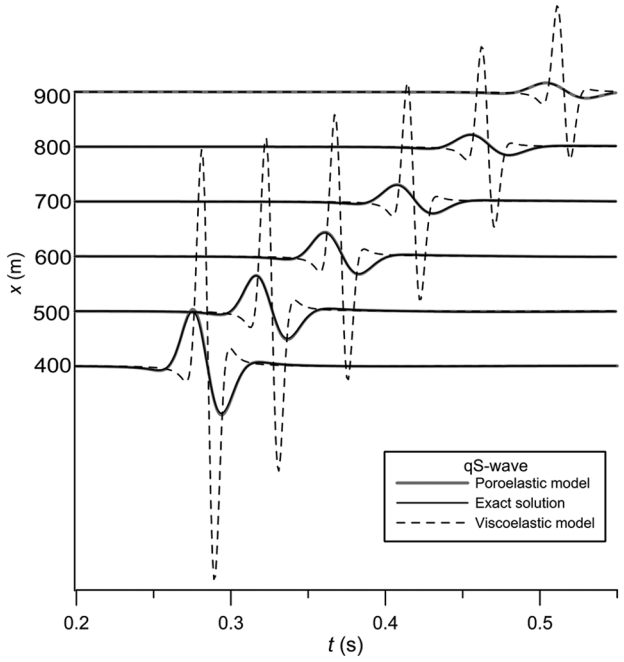

Figure 8. The qS-waveforms at a depth $z = 100$ m for different x. The medium consists of the layers of coarse sand, $l_1 = 0.09$ m (water saturated), $l_2 = 0.01$ m (gas saturated), $f_R = 50$ Hz. The actual arrival times are not shown here, and the interval between the arrival times $t = 0.04$ s is chosen for visualization purposes. The traces predicted by the effective viscoelastic model are scaled by the factor 0.5.

However, Biot's global flow mechanism is not captured by the viscoelastic model; this is why the model gives inaccurate predictions. Clearly, the attenuation caused by Biot's global flow mechanism is not negligible at low frequencies for highly permeable media. The difference in the qS-waveforms predicted by the effective poroelastic model and the exact solution, which changes with offset, suggests again that the mesoscopic-scale attenuation mechanism incorporated in the model via the effective frequency-dependent elastic moduli derived from the 1D cell problem fails to predict the qS-wave attenuation with high accuracy.

The attenuation of seismic waves is known to be very pronounced in finely layered porous media with patchy saturation (Carcione and Picotti, 2006). The next example is a finely layered coarse sand saturated with water and gas. The layer thicknesses are $l_1 = 0.09$ m (water saturated) and $l_2 = 0.01$ m (gas saturated). The vertical distance from the source to the receivers is $z = 100$ m. The wavelet's central frequency $f_R = 50$ Hz. The time-domain responses for the horizontal line of receivers are depicted in Figure 7 (qP-wave) and Figure 8 (qS-wave). The horizontal positions of the receivers are chosen differently than in the previous examples, for visualization purposes (the medium is highly attenuative). Clearly, the effective viscoelastic model vastly underestimates the attenuation, to a much greater extent than in the previous examples, whereas the effective poroelastic model is in good agreement with the exact solution. The effective viscoelastic model also predicts lower qP-wave velocities than the poroelastic model and the exact solution, as can be seen in Figure 7. The waveforms predicted by the effective viscoelastic model are also different, suggesting that the dispersion is not captured properly. It can be observed in the (f, k_x) domain that the effective poroelastic model (Figure 9a) and the exact solution (Figure 9b) are in good agreement, whereas the amplitudes predicted by the effective viscoelastic model (Figure 9c) are much higher and the P-wave velocity is lower.

Because highly permeable media are highly dispersive and attenuative, it is interesting to explore the angle-dependent effects in more detail with the configuration of receivers depicted in Figure 1b. The distance from source to the receivers is $r = 100$ m. The results for this configuration are depicted in Figures 10 and 11. In these plots, the time-domain responses are shown for the locations of receivers at different angles θ. The results for the qP-wave are depicted in Figure 10. The deviation of the predictions of the effective viscoelastic model from the exact result is visible even at normal incidence; this

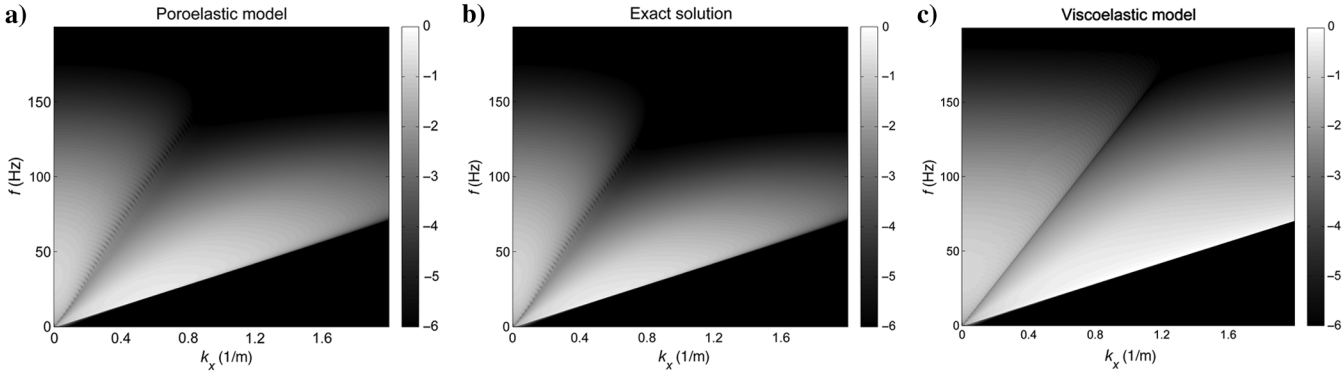

Figure 9. Logarithm of the amplitude spectrum in the (f, k_x)-domain for the vertical component of solid particle displacement at a depth $z = 100$ m. Water- and gas-saturated coarse sand.

result is consistent with that obtained by Kudarova et al. (2013). The effective poroelastic model predicts the same attenuation and dispersion as the exact solution. It can be observed in Figure 10 that the effective viscoelastic model does not correctly predict the angle-dependent dispersion of this medium. There is a significant phase shift between the predictions of the viscoelastic and poroelastic solutions, observed by the change in the waveform. The dispersion effects are very pronounced in the effective poroelastic model and the exact solution: with increasing angle, the waveform spreads.

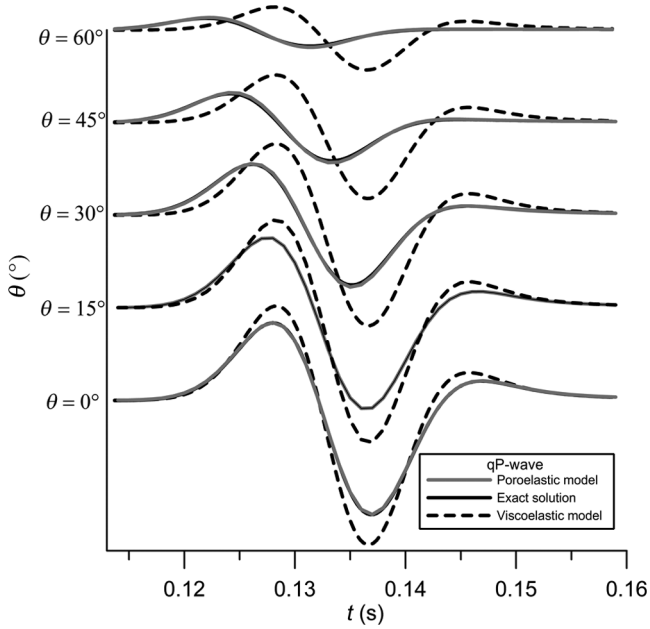

Figure 10. The qP-waveforms at a distance $r = 100$ m from the source at different angles. The medium consists of the layers of coarse sand, $l_1 = 0.09$ m (water saturated), $l_2 = 0.01$ m (gas saturated), $f_R = 50$ Hz. Solid gray and black lines coincide.

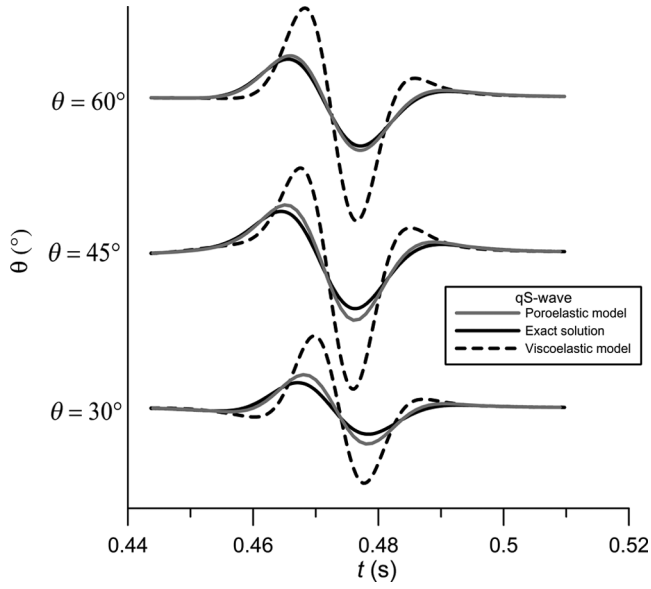

Figure 11. The qS-waveforms at a distance $r = 100$ m from the source at different angles. The medium consists of the layers of coarse sand, $l_1 = 0.09$ cm (water saturated), $l_2 = 0.01$ m (gas saturated), $f_R = 50$ Hz.

There is again some difference in the predictions of the effective poroelastic model and the exact solution for the qS-wave as can be seen in Figure 11. In these highly dispersive media, the qS-wave attenuation due to the mesosocopic-scale wave-induced fluid flow is more significant than in less permeable stiffer rocks. However, as mentioned above, the S-wave attenuation and dispersion due to mesosocopic effects is not fully correctly described by the effective models. Still, the effective poroelastic model gives better predictions of the qS-wave attenuation than the viscoelastic model.

In this section, we have observed that the qP- and qS-waveforms are predicted accurately for rocks 1 and 2 (Figure 2), where the influence of Biot's global flow mechanism is negligible, and the mesoscopic-scale attenuation mechanism is captured properly by the effective moduli in both models. The differences in qS-waveforms are more pronounced with increasing the frequency and for softer sandstones (Figure 4). Biot's global flow mechanism becomes nonnegligible for unconsolidated sands (Figures 5–11), resulting in underestimation of qP- and qS-waves attenuation by the effective viscoelastic model; however, the poroelastic model predicts the proper qP-wave attenuation for such materials, whereas the qS-wave attenuation has higher accuracy than that predicted by the viscoelastic model.

DISCUSSION

The effective models discussed in this paper are based on the assumption that the direction of fluid flow is always perpendicular to the layering. The frequency-dependent functions in both effective models describe the attenuation due to interlayer flow at normal incidence. It was shown in this study that this assumption is reasonable for qP-waveforms. The predictions by the effective poroelastic model are in good agreement with the predictions by the exact solution. Predictions by the effective viscoelastic model are in agreement with the exact solution only in situations in which Biot's global flow mechanism is not significant.

The exact solution is readily available for periodically layered media. One may question the justification of the development of effective models for such configurations. However, it is much easier to work with effective homogenized equations giving simpler expressions. The model of White et al. (1975) is an example; many publications report on studies with this model already for decades. The effective models for periodic structures can in many cases be extended to the nonperiodic case to handle more complicated geometries. The exact analytical solution available for periodically distributed inclusions validates the methods used to obtain the effective models. Although only 2D numerical examples were shown, the models discussed in this paper can be used to solve problems in

Table 2. Mechanical properties of the sample pore fluids.

Parameter	Notation	Units	Water	Gas	CO_2
Density	ρ_f	kg/m^3	1000	140	505
Bulk modulus	K_f	GPa	2.25	0.056	0.025
Viscosity	η	Pa*s	0.001	0.00022	0.00015

3D and can be extended to the situation of nonperiodic layering when different frequency-dependent relaxation functions are used (derived for a nonperiodic case).

Viscoelastic models are often advantageous over the poroelastic ones because they require fewer parameters and improve computational efficiency. However, poroelastic models are required for predictions of frequency-dependent attenuation in highly permeable media, such as shallow marine sediments with an inhomogeneous frame and partial saturation, and unconsolidated sand reservoirs.

CONCLUSION

Finely layered porous media can be highly dispersive and attenuative, for example, due to the variations in the properties of saturating fluids, the presence of soft layers and fractures. In this paper, a new effective poroelastic model is proposed for wave propagation in such layered porous media. In this new model, the attenuation of seismic waves at mesoscopic scale is described by three frequency-dependent relaxation functions, which were computed for P-waves at normal incidence. The extension to the angle-dependent propagation is provided by the use of poroelastic Backus averaging. The effective models (the viscoelastic and the poroelastic one) are validated with the exact analytical solution obtained with the use of Floquet's theory applied to Biot's equations with periodically varying coefficients. The effective models predict different qP-wave attenuation and dispersion for soft unconsolidated layers. This is explained by the fact that Biot's global flow attenuation mechanism is not included in the effective viscoelastic model. The examples show that the effective poroelastic model predicts the qP-waveform with high accuracy.

There is a major difference in the predictions of qS-wave attenuation by the effective viscoelastic model and the newly introduced poroelastic model. The effective viscoelastic model predicts mesoscopic attenuation of qS-waves due to the coupling between P- and S-wave motions. The effective medium is isotropic when the shear modulus is constant; then, there is no coupling between P- and S-wave motions. In this case, the S-wave in the effective viscoelastic model is lossless. However, the effective poroelastic model predicts mesoscopic S-wave attenuation even for constant shear modulus; in addition, there is attenuation due to Biot's global flow. The numerical examples show that this results in a perceptible differences between the waveforms predicted by the effective viscoelastic and poroelastic models, and that the predictions by the effective poroelastic model are much closer to the exact result.

We conclude that the method used for extension of the attenuation and dispersion caused by the interlayer flow in 1D to the arbitrary angle of incidence provides a very good match between the resulting effective model and the exact solution, especially for the qP-wave. The effective poroelastic VTI model, introduced in this paper, is advantageous when soft unconsolidated layers are present. It is also applicable at a broader frequency range than the effective viscoelastic model.

ACKNOWLEDGMENTS

This research was carried out in the context of the CATO-2-program. CATO-2 is the Dutch National Research Program on CO_2 capture and storage technology. The program is financially supported by the Dutch government and the CATO-2 Consortium parties. The second author was sponsored by the Research Centre for Integrated Solid Earth Science.

APPENDIX A

ANALYTICAL SOLUTION FOR PERIODICALLY LAYERED POROUS MEDIUM

The solution of first-order differential equations with periodic coefficients can be obtained using Floquet's (1883) theorem. This theory is extensively used in numerous applications in different disciplines. In particular, it has been applied to elastic composites by Braga and Hermann (1992) and to a 1D poroelastic composite by Norris (1993) and Kudarova et al. (2013). In this appendix, we apply the method to a 2D poroelastic composite to obtain an analytical solution that will be used to validate the effective models. The procedure is outlined below.

We consider a periodically layered medium consisting of alternating layers 1 and 2, with the thicknesses l_1 and l_2, and the period $L = l_1 + l_2$ (see Figure 1a). Each layer is described by Biot's equations of poroelasticity (equations 1 and 2), and each layer is isotropic. The equations of motion (equations 1 and 2), with the stress-strain relations (equation 5) substituted, can in the frequency-wavenumber domain be written in the matrix notation:

$$\frac{\partial \hat{\mathbf{f}}}{\partial z} = \mathrm{i}\hat{\mathbf{N}}\hat{\mathbf{f}}, \tag{A-1}$$

where $\hat{\mathbf{N}}$ is a matrix given in Appendix B; $\hat{\mathbf{f}} = [\hat{v}_z, \hat{\xi}_z, \hat{\sigma}_{xz}, \hat{\sigma}_{zz}, \hat{p}, \hat{v}_x]$ is a vector-containing field variables; $\hat{v}_z$ and $\hat{v}_x$ are the z- and x-components of the solid particle velocity, respectively; $\hat{\xi}_z = (1-\phi)\hat{v}_z + \phi\hat{v}_z^f$, where $\hat{v}_z^f$ is a vertical component of the fluid particle velocity; $\hat{\sigma}_{xz} = -\hat{\tau}_{xz}$ and $\hat{\sigma}_{zz} = -\hat{\tau}_{zz} - \hat{p}$ are the intergranular stresses.

The elements of the matrix $\hat{\mathbf{N}}$ are periodic functions of the vertical coordinate z (with the period L) and depend on frequency ω and horizontal slowness $s_x = k_x/\omega$. According to Floquet (1883), the solution of equation A-1 can be found in the form

$$\hat{\mathbf{f}} = \hat{\mathbf{Y}}(z)\mathbf{c}, \qquad \hat{\mathbf{Y}} = \hat{\mathbf{F}}(z)\exp(\mathrm{i}\hat{\mathbf{A}}z), \tag{A-2}$$

where $\mathbf{c}$ is a vector containing six constants to be defined by the boundary conditions and matrix $\hat{\mathbf{F}}(z)$ is a periodic matrix, $\hat{\mathbf{F}}(z) = \hat{\mathbf{F}}(z+L)$; matrix $\hat{\mathbf{A}}$ is constant with respect to z. To find the matrices $\hat{\mathbf{F}}$ and $\hat{\mathbf{A}}$, let us consider the solution of equation A-1 within one period L that consists of two layers and is referred to as a periodic cell.

For a stack of layers, the solution of equation A-1 can be expressed via the propagator matrix $\hat{\mathbf{P}}(z)$: $\hat{\mathbf{f}}(z) = \hat{\mathbf{P}}(z)\hat{\mathbf{f}}(z_0)$, where z_0 is the vertical coordinate of the top interface. It follows from this expression that $\hat{\mathbf{P}}(z_0) = \mathbf{I}$, where $\mathbf{I}$ is the identity matrix. Using Floquet's solution equation A-2 at $z = z_0$, one finds $\hat{\mathbf{f}}(z_0) = \hat{\mathbf{F}}(z_0)\exp(\mathrm{i}\hat{\mathbf{A}}z_0)\hat{\mathbf{f}}(z_0)$, and consequently, $\hat{\mathbf{F}}(z_0)\exp(\mathrm{i}\hat{\mathbf{A}}z_0) = \mathbf{I}$. From this relation and the periodicity of $\hat{\mathbf{F}}(z)$, it follows that

$$\hat{\mathbf{f}}(z_0+L) = \hat{\mathbf{F}}(z_0)\exp(\mathrm{i}\hat{\mathbf{A}}z_0)\exp(\mathrm{i}\hat{\mathbf{A}}L)\hat{\mathbf{f}}(z_0) = \exp(\mathrm{i}\hat{\mathbf{A}}L)\hat{\mathbf{f}}(z_0). \tag{A-3}$$

On the other hand, using the propagator matrix, we have $\hat{\mathbf{f}}(z_0+L) = \hat{\mathbf{P}}(z_0+L)\hat{\mathbf{f}}(z_0)$. Hence, $\hat{\mathbf{P}}(z_0+L) = \exp(\mathrm{i}\hat{\mathbf{A}}L)$.

Let us now consider the solution for the two layers of the periodic cell with the coordinates $z_0 \le z \le z_0 + l_1$ for layer 1 and $z_0 + l_1 \le$

$z \le z_0 + L$ for layer 2. In each of the layers 1 and 2, the solution of equation A-1 is

$$\hat{\mathbf{f}}_k(z) = \hat{\mathbf{M}}_k(z)\hat{\mathbf{f}}(z_k), \quad k = 1,2,$$
$$\hat{\mathbf{M}}_k(z) = \exp(\mathrm{i}\hat{\mathbf{N}}_k z), \quad \hat{\mathbf{M}}_k(z_k) = \mathbf{I}, \tag{A-4}$$

where z_k is the vertical coordinate of the top interface of the layer k. Following this solution, $\hat{\mathbf{f}}(z_0 + l_1) = \hat{\mathbf{M}}_1(l_1)\hat{\mathbf{f}}(z_0)$ and $\hat{\mathbf{f}}(z_0 + L) = \hat{\mathbf{M}}_2(l_2)\hat{\mathbf{f}}(z_0 + l_1) = \hat{\mathbf{M}}_2(l_2)\hat{\mathbf{M}}_1(l_1)\hat{\mathbf{f}}(z_0)$. Hence,

$$\hat{\mathbf{P}}(z_0 + L) = \exp(\mathrm{i}\hat{\mathbf{A}}L) = \exp(\mathrm{i}\hat{\mathbf{N}}_2 l_2)\exp(\mathrm{i}\hat{\mathbf{N}}_1 l_1). \tag{A-5}$$

Matrix $\hat{\mathbf{A}}$ is now defined via the relation of the matrix exponentials in equation A-5. The eigenvalues of the matrix $\hat{\mathbf{A}}$ are the so-called Floquet wavenumbers that govern the wave propagation in periodic media. The first step in finding these wavenumbers is to find the matrix exponentials $\exp(\mathrm{i}\hat{\mathbf{N}}_k l_k)$, $k = 1,2$. To compute this matrix, it is convenient to use the eigendecomposition $\hat{\mathbf{N}}_k = \hat{\mathbf{L}}_k\hat{\mathbf{\Lambda}}_k\hat{\mathbf{L}}_k^{-1}$, where $\hat{\mathbf{L}}_k$ is a matrix containing the eigenvectors of the matrix $\hat{\mathbf{N}}_k$ and $\hat{\mathbf{\Lambda}}_k$ is a diagonal matrix containing its eigenvalues, which are the vertical components of the wavenumbers governing wave propagation inside the layer:

$$k_{1z}^{\pm} = \pm\omega\sqrt{\frac{-\hat{d}_1 - \sqrt{\hat{d}_1^2 - 4\hat{d}_0 d_2}}{2d_2} - s_x^2},$$
$$k_{2z}^{\pm} = \pm\omega\sqrt{\frac{-\hat{d}_1 + \sqrt{\hat{d}_1^2 - 4\hat{d}_0 d_2}}{2d_2} - s_x^2},$$
$$k_{3z}^{\pm} = \pm\omega\sqrt{\frac{\hat{d}_0}{\mu\hat{\rho}_{22}} - s_x^2}, \tag{A-6}$$

where $\hat{d}_0 = \hat{\rho}_{11}\hat{\rho}_{22} - \hat{\rho}_{12}^2$, $\hat{d}_1 = -(P\hat{\rho}_{22} + R\hat{\rho}_{11} - 2Q\hat{\rho}_{12})$, $d_2 = PR - Q^2$, and the density terms $\hat{\rho}_{ij}$ are defined in Appendix B. The vertical wavenumbers in equation A-6 correspond to the upgoing, downgoing fast, slow P-, and S-waves. The elements of the matrices $\hat{\mathbf{L}}_k$ are not explicitly presented here for the sake of brevity. They are expressed via the elements of the matrices $\hat{\mathbf{N}}_k$ and can be found using the eigendecomposition. The vertical components of the Floquet wavenumbers k_{iz}^F are expressed via the eigenvalues τ_i of the matrix $\exp(\mathrm{i}\hat{\mathbf{A}}L)$: $\tau_i = \exp(\mathrm{i}k_{iz}^F L)$.

The next step toward obtaining the solution of equation A-1 is to find the periodic matrix $\hat{\mathbf{F}}(z)$. Without loss of generality, we assume the coordinate of the top interface $z_0 = 0$. Let us define the local coordinate $z_n = z - (n-1)L$, where n is the number of the periodic cell and $0 \le z_n \le L$. Then, the following equalities hold:

$$\hat{\mathbf{P}}(z) = \hat{\mathbf{F}}(z)\exp(\mathrm{i}\hat{\mathbf{A}}z) = \hat{\mathbf{F}}(z_n)\exp(\mathrm{i}\hat{\mathbf{A}}z_n)\exp(\mathrm{i}\hat{\mathbf{A}}L(n-1))$$
$$= \hat{\mathbf{P}}(z_n)\exp(\mathrm{i}\hat{\mathbf{A}}L(n-1)). \tag{A-7}$$

Right-multiplying equation A-7 by $\exp(-\mathrm{i}\hat{\mathbf{A}}z)$ results in the expression

$$\hat{\mathbf{F}}(z) = \hat{\mathbf{P}}(z_n)\exp(-\mathrm{i}\hat{\mathbf{A}}z_n), \tag{A-8}$$

where the propagator matrix $\hat{\mathbf{P}}(z_n)$ is defined as

$$\hat{\mathbf{P}}(z_n) = \begin{cases} \hat{\mathbf{M}}_1(z_n), & 0 \le z_n \le l_1, \\ \hat{\mathbf{M}}_2(z_n - l_1)\hat{\mathbf{M}}_1(l_1), & l_1 \le z_n \le L. \end{cases} \tag{A-9}$$

The matrices $\hat{\mathbf{F}}$ and $\hat{\mathbf{A}}$ have been determined in equations A-5 and A-8, and the solution of equation A-1 can now be obtained:

$$\hat{\mathbf{f}}(z) = \hat{\mathbf{F}}(z)\exp(\mathrm{i}\hat{\mathbf{A}}z)\hat{\mathbf{f}}(0) = \hat{\mathbf{P}}(z_n)\exp(\mathrm{i}\hat{\mathbf{A}}L(n-1))\hat{\mathbf{f}}(0). \tag{A-10}$$

The vector $\hat{\mathbf{f}}(0)$ is the solution of Biot's equations related to the top layer:

$$\hat{\mathbf{f}}(z_0) = \hat{\mathbf{S}}[A_1 \quad A_2 \quad A_3 \quad A_4 \quad A_5 \quad A_6]^{\mathrm{T}}. \tag{A-11}$$

The elements of matrix $\hat{\mathbf{S}}$ are given in Appendix B. The unknown amplitudes A_i are defined by the boundary conditions. In the examples that follow, we consider the half-space subject to a point-source $\tau_{zz} = f(t)\delta(x)$ at the top interface. In this case, the following six boundary conditions are applied: At the top interface $z = 0$, the stress σ_{zz} is continuous, $\sigma_{zx} = 0$, fluid pressure $p = 0$, and the radiation condition, which implies the absence of all three upgoing waves.

APPENDIX B

MATRICES OF COEFFICIENTS IN THE ANALYTICAL SOLUTION

The matrix of coefficients $\hat{\mathbf{N}}$ in the equations A-1 reads

$$\hat{\mathbf{N}} = \omega\begin{bmatrix} \mathbf{0} & \hat{\mathbf{N}}^a \\ \hat{\mathbf{N}}^b & \mathbf{0} \end{bmatrix},$$

$$\hat{\mathbf{N}}^a = \begin{bmatrix} -\frac{R}{d_2} & \phi\frac{Q'}{d_2} & s_x\left(1 - \frac{2\mu R}{d_2}\right) \\ .. & \frac{s_x^2\phi^2}{\hat{\rho}_{22}} - \frac{\phi(\phi P - (1-\phi)Q)}{d_2} + \frac{\phi(1-\phi)Q'}{d_2} & s_x\left(1 - \phi - \phi\frac{\hat{\rho}_{12}}{\hat{\rho}_{22}} + \frac{2\mu\phi Q'}{d_2}\right) \\ .. & .. & 4\mu s_x^2\left(1 - \frac{\mu R}{d_2}\right) + \frac{\hat{\rho}_{12}^2}{\hat{\rho}_{22}} - \hat{\rho}_{11} \end{bmatrix},$$

$$\hat{\mathbf{N}}^b = \begin{bmatrix} \frac{2\hat{\rho}_{12}(1-\phi)}{\phi} - \frac{\hat{\rho}_{22}(1-\phi)^2}{\phi^2} - \hat{\rho}_{11} & \frac{\hat{\rho}_{22}(1-\phi)}{\phi^2} - \frac{\hat{\rho}_{12}}{\phi} & s_x \\ .. & -\frac{\hat{\rho}_{22}}{\phi^2} & 0 \\ .. & .. & -\frac{1}{\mu} \end{bmatrix}, \tag{B-1}$$

where the dots denote the elements below the diagonal, which are equal to the corresponding elements above the diagonal because matrices $\hat{\mathbf{N}}^a$ and $\hat{\mathbf{N}}^b$ are symmetric. In the elements of $\hat{\mathbf{N}}$, $s_x = k_x/\omega$ is the horizontal slowness, $\hat{\rho}_{12} = -(\alpha_\infty - 1)\phi\rho_f + \mathrm{i}\hat{b}/\omega$, $\hat{\rho}_{11} = (1-\phi)\rho_s - \hat{\rho}_{12}$, and $\hat{\rho}_{22} = \phi\rho_f - \hat{\rho}_{12}$. The damping operator $\hat{b} = b_0\sqrt{1 + \mathrm{i}\omega/(2\omega_B)}$, where $b_0 = \eta\phi^2/k_0$. The coefficients $d_2 = PR - Q^2$, $Q' = Q - (1-\phi)R/\phi$.

The elements of the matrix $\hat{\mathbf{S}}$ from equation A-11 read $\hat{S}_{ij} = \hat{g}_i(k_{jz}^{\pm})$, where $k_{jz}^{\pm}$, $j = 1,..,6$ are the six wavenumbers defined in equation A-6. The functions $\hat{g}_i(k_z)$, $i = 1,6$ read

$$\hat{g}_1 = \mathrm{i}\omega,\ \hat{g}_2 = \mathrm{i}\omega(1+\beta_{zf}),$$
$$\hat{g}_3 = -\mathrm{i}(1-\phi)E_3(k_z\beta_{zf}+k_x\beta_{xf})+\mathrm{i}(\mu k_z-(1-\phi)E_2k_x)\beta_x - \mathrm{i}(E_2k_z+\mu k_x),$$
$$\hat{g}_4 = \mathrm{i}((E_1-2\mu)k_x-(1-\phi)E_2k_x)(\beta_x+\mathrm{i}(E_2-(1-\phi)E_3) \times(\beta_{xf}k_x+\beta_{zf}k_z)+\mathrm{i}k_z(E_1-(1-\phi)E_2),$$
$$\hat{g}_5 = \mathrm{i}E_2(k_z+\beta_xk_x)+E_3(k_z\beta_{zf}+k_x\beta_{xf}),\ \hat{g}_6 = \mathrm{i}\omega\beta_x. \quad \text{(B-2)}$$

The coefficients β_{zf}, β_{xf}, and β_x are the ratios of the amplitudes $\hat{W}_z$, $\hat{W}_x$, and $\hat{U}_x$ from equation 7 to $\hat{U}_z$, respectively. They read

$$\beta_x = -\frac{\hat{m}k_xk_z}{\Delta}(\omega^2(E_2\rho_f+\hat{m}(\mu-E_1))+k_z^2(E'-\mu E_3),$$
$$\beta_{zf} = -\frac{1}{\Delta}(\omega^4\hat{m}'-\omega^2((\hat{m}\mu\rho_f+\hat{m}'E_2)k_z^2+\rho_fk_x^2(\rho_fE_2-\hat{m}E_1))+ +\hat{m}\mu E_2k_z^4+(\mu(\hat{m}E_2-\rho_fE_3)+E'\rho_f)k_z^2k_x^2),$$
$$\Delta = \hat{m}\omega^4\hat{m}'-\omega^2((\hat{m}'E_3+\hat{m}^2\mu)k_z^2+\hat{m}(\hat{m}E_1-\rho_fE_2)k_x^2) +\hat{m}k_z^2(\mu E_3k_z^2+E'k_x^2),$$
$$\beta_{xf} = -\frac{\rho_f}{\hat{m}}\beta_x,\quad \hat{m}' = \hat{m}\rho-\rho_f^2,\ E' = E_1E_3-E_2^2. \quad \text{(B-3)}$$

APPENDIX C

FORMULAS FOR THE EFFECTIVE VISCOELASTIC VTI MEDIUM

The formulas for relaxed and unrelaxed elastic coefficients used by Krzikalla and Müller (2011) and used in this paper were originally derived by Gelinsky and Shapiro (1997). The unrelaxed coefficients read

$$A^u = \left\langle\frac{4\mu(\lambda^u+\mu)}{P^u}\right\rangle+\left\langle\frac{1}{P^u}\right\rangle^{-1}\left\langle\frac{\lambda^u}{P^u}\right\rangle^2,$$
$$C^u = \left\langle\frac{1}{P^u}\right\rangle^{-1},\quad F^u = \left\langle\frac{1}{P^u}\right\rangle^{-1}\left\langle\frac{\lambda^u}{P^u}\right\rangle,\quad D^u = \left\langle\frac{1}{\mu}\right\rangle^{-1},$$
$$B_6^u = B_7^u = \left\langle\frac{\frac{1-\phi}{K_s}-\frac{K_b}{K_s^2}+\frac{\phi}{K_f}}{(1-\frac{K_b}{K_s})}\right\rangle^{-1}. \quad \text{(C-1)}$$

In equation C-1,

$$\lambda^u = K_b-\frac{2}{3}\mu+\left(1-\frac{K_b}{K_s}\right)^2\left(\frac{1-\phi}{K_s}-\frac{K_b}{K_s^2}+\frac{\phi}{K_f}\right)^{-1},$$
$$P^u = \lambda^u+2\mu. \quad \text{(C-2)}$$

The unrelaxed limit of B_8 is not defined because this coefficient is not present in the stress-strain relations because $\nabla\mathbf{w}=\mathbf{0}$ (the no-flow condition; see Gelinsky and Shapiro, 1997). The relaxed coefficients read

$$A^r = \left\langle\frac{4\mu(\lambda^r+\mu)}{P^r}\right\rangle+\left\langle\frac{1}{P^r}\right\rangle^{-1}\left\langle\frac{\lambda}{P^r}\right\rangle^2+\frac{(B_6^r)^2}{B_8^r},$$
$$C^r = \left\langle\frac{1}{P^r}\right\rangle^{-1}+\frac{(B_7^r)^2}{B_8^r},\quad F^u = \left\langle\frac{1}{P^r}\right\rangle^{-1}\left\langle\frac{\lambda^r}{P^r}\right\rangle+\frac{B_6^rB_7^r}{B_8^r},\quad D^u = \left\langle\frac{1}{\mu}\right\rangle^{-1},$$
$$B_6^r = -B_8^r\left(\left\langle\frac{2(1-\frac{K_b}{K_s})\mu}{P^r}\right\rangle+\left\langle\frac{1-\frac{K_b}{K_s}}{P^r}\right\rangle\left\langle\frac{\lambda^r}{P^r}\right\rangle\left\langle\frac{1}{P^r}\right\rangle^{-1}\right),$$
$$B_7^r = -B_8^r\left\langle\frac{1-\frac{K_b}{K_s}}{P^r}\right\rangle\left\langle\frac{1}{P^r}\right\rangle^{-1},$$
$$B_8^r = \left(\left\langle\frac{1-\phi}{K_s}-\frac{K_b}{K_s^2}+\frac{\phi}{K_f}\right\rangle+\left\langle\frac{(1-\frac{K_b}{K_s})^2}{P^r}\right\rangle-\left\langle\frac{1-\frac{K_b}{K_s}}{P^r}\right\rangle^2\left\langle\frac{1}{P^r}\right\rangle^{-1}\right)^{-1}. \quad \text{(C-3)}$$

In equation C-3,

$$\lambda^r = K_b-\frac{2}{3}\mu,\qquad P^r = \lambda^r+2\mu. \quad \text{(C-4)}$$

The frequency-dependent plane-wave modulus that connects the relaxed and unrelaxed regimes (see equation 14) was derived by White et al. (1975). It is defined by the following relations:

$$\hat{c}(\omega) = \frac{c^*}{1+2(R_1-R_2)^2\mathrm{i}/(\omega L(Z_1+Z_2))},\quad c^* = \langle(P^u)^{-1}\rangle^{-1}, \quad \text{(C-5)}$$

where for each layers 1 and 2

$$R = \left(1-\frac{K_b}{K_s}\right)\frac{K_a}{P_u},\quad K_a = \left(\frac{1-\phi}{K_s}-\frac{K_b}{K_s^2}+\frac{\phi}{K_f}\right)^{-1},$$
$$Z = Z_0\cot\left(\frac{1}{2}\alpha_wl\right),\quad Z_0 = \sqrt{\eta K_e\mathrm{i}/(\omega k_0)},$$
$$\alpha_w = \sqrt{-\mathrm{i}\omega\eta/(k_0K_e)},\quad K_e = K_a\left(K_b+\frac{4}{3}\mu\right)/P^u. \quad \text{(C-6)}$$

REFERENCES

Biot, M. A., 1962, Mechanics of deformation and acoustic propagation in porous media: Journal of Applied Physics, **33**, 1482–1498, doi: 10.1063/1.1728759.

Braga, A. B., and G. Hermann, 1992, Floquet waves in anisotropic layered composites: Journal of the Acoustical Society of America, **91**, 1211–1227, doi: 10.1121/1.402505.

Brajanovski, M., and B. Gurevich, 2005, A model for P-wave attenuation and dispersion in a porous medium permeated by aligned fractures: Geophysical Journal International, **163**, 372–384, doi: 10.1111/gji.2005.163.issue-1.

Carcione, J. M., and S. Picotti, 2006, P-wave seismic attenuation by slow-wave diffusion: Effects of inhomogeneous rock properties: Geophysics, **71**, no. 3, O1–O8, doi: 10.1190/1.2194512.

Carcione, J. M., J. E. Santos, and S. Picotti, 2011, Anisotropic poroelasticity and wave-induced fluid flow: Harmonic finite-element simulations: Geophysical Journal International, **186**, 1245–1254, doi: 10.1111/j.1365-246X.2011.05101.x.

Dvorkin, J., and A. Nur, 1993, Dynamic poroelasticity: A unified model with the squirt and the Biot mechanisms: Geophysics, **58**, 524–533, doi: 10.1190/1.1443435.

Floquet, G., 1883, Sur les équations différentielles linéaires à coefficients périodiques: Annales scientifiques de l'École Normale Supérieure, **2**, 47–88.

Gelinsky, S., and S. A. Shapiro, 1997, Poroelastic Backus averaging for anisotropic layered fluid- and gas-saturated sediments: Geophysics, **62**, 1867–1878, doi: 10.1190/1.1444287.

Gelinsky, S., S. A. Shapiro, T. Müller, and B. Gurevich, 1998, Dynamic poroelasticity of thinly layered structures: International Journal of Solids and Structures, **35**, 4739–4751, doi: 10.1016/S0020-7683(98)00092-4.
Gist, G. A., 1994, Interpreting laboratory velocity measurements in partially gas-saturated rocks: Geophysics, **59**, 1100–1109, doi: 10.1190/1.1443666.
Johnson, D. L., 2001, Theory of frequency dependent acoustics in patchy-saturated porous media: Journal of the Acoustical Society of America, **110**, 682–694, doi: 10.1121/1.1381021.
Johnson, D. L., J. Koplik, and R. Dashen, 1987, Theory of dynamic permeability and tortuosity in fluid-saturated porous media: Journal of Fluid Mechanics, **176**, 379–402, doi: 10.1017/S0022112087000727.
Johnston, D. H., M. N. Toksöz, and A. Timur, 1979, Attenuation of seismic waves in dry and saturated rocks: mechanisms: Geophysics, **44**, 691–711, doi: 10.1190/1.1440970.
Krzikalla, F., and T. M. Müller, 2011, Anisotropic P-SV-wave dispersion and attenuation due to inter-layer flow in thinly layered porous rocks: Geophysics, **76**, no. 3, WA135–WA145, doi: 10.1190/1.3555077.
Kudarova, A. M., K. N. van Dalen, and G. G. Drijkoningen, 2013, Effective poroelastic model for one-dimensional wave propagation in periodically layered media: Geophysical Journal International, **195**, 1337–1350, doi: 10.1093/gji/ggt315.
Mavko, G., and A. Nur, 1979, Wave propagation in partially saturated rocks: Geophysics, **44**, 161–178, doi: 10.1190/1.1440958.
Molotkov, L. A., and A. V. Bakulin, 1999, Effective models of stratified media containing porous Biot layers: Journal of Mathematical Sciences, 3385–3371 ,**96**, doi: 10.1007/BF02172816.
Müller, T. M., B. Gurevich, and M. Lebedev, 2010, Seismic wave attenuation and dispersion resulting from wave-induced flow in porous rocks — A review: Geophysics, **75**, no. 5, A147–A164, doi: 10.1190/1.3463417.
Norris, A., 1993, Low-frequency dispersion and attenuation in partially saturated rocks: Journal of the Acoustical Society of America, **94**, 359–370, doi: 10.1121/1.407101.
O'Connell, R. J., and B. Budiansky, 1977, Visco-elastic properties of fluid-saturated cracked solids: Journal of Geophysical Research, **82**, 5719–5735, doi: 10.1029/JB082i036p05719.
Palmer, I. D., and M. L. Traviola, 1980, Attenuation by squirt flow in undersaturated gas sands: Geophysics, **45**, 1780–1792, doi: 10.1190/1.1441065.
Smeulders, D. M. J., R. L. G. M. Eggels, and M. E. H. van Dongen, 1992, Dynamic permeability: Reformulation of theory and new experimental and numerical data: Journal of Fluid Mechanics, **245**, 211–227, doi: 10.1017/S0022112092000429.
Turgut, A., and T. Yamamoto, 1990, Measurements of acoustic wave velocities and attenuation in marine sediments: Journal of the Acoustical Society of America, **87**, 2376–2383, doi: 10.1121/1.399084.
Vogelaar, B., and D. Smeulders, 2007, Extension of White's layered model to the full frequency range: Geophysical Prospecting, **55**, 685–695, doi: 10.1111/gpr.2007.55.issue-5.
Wenzlau, F., J. B. Altmann, and T. M. Müller, 2010, Anisotropic dispersion and attenuation due to wave-induced fluid flow: Quasi-static finite element modeling in poroelastic solids: Journal of Geophysical Research, **115**, B07204, doi: 10.1029/2009JB006644.
White, J. E., N. G. Mikhaylova, and F. M. Lyakhovistkiy, 1975, Low-frequency seismic waves in fluid saturated layered rocks: Physics of Solid Earth, **11**, 654–659.
Winkler, K., 1985, Dispersion analysis of velocity and attenuation in Berea sandstone: Journal of Geophysical Research, **90**, 6793–6800, doi: 10.1029/JB090iB08p06793.